

Laser Gyroscope

A249 - Course Description

Thorsten Groh, Jannik Zenner and Simon Stellmer

2021-08-01

Contents

1 Literature	2
2 Outline of the course	2
3 Background information	2
3.1 Prelude: The rotation of Earth	2
3.2 Gyroscopes based on the Sagnac effect	5
3.2.1 The Sagnac effect	5
3.2.2 Early gyroscopes: the Michelson-Gale experiment	6
3.2.3 Active ring laser gyroscopes	7
3.2.4 Passive ring laser gyroscopes	10
3.3 Fundamentals of optical cavities	10
3.3.1 Cavity modes	10
3.3.2 Finesse	12
3.3.3 Pound-Drever-Hall locking	13
3.3.4 The lock-in effect	14
3.4 Quantifying performance: the Allan deviation	16
4 The setup	17
5 The lab course	22
5.1 Homework preparation	22
5.2 Laboratory tasks	23
References	27

1 Literature

As preparation for the oral exam and for conduction of the experiment, please **read and understand** this **course description**, as well as the publication **Optics Letters 44, 2732 (2019)** [4]. Additional information to deepen your understanding of the topics can be found in the references and in the literature folder on sciebo.

2 Outline of the course

In this lab course experiment you will learn about gyroscopes and study the relativistic Sagnac effect using a passive free-space laser gyroscope.

In your preparation homework you will dive into the topic of rotation measurements by reading out the built-in gyroscope of your phone using the phyphox app. You will learn how to characterize these type of devices and identify their limits. Furthermore you will attempt a measurement of the rotation rate of Earth.

In the laboratory experiment part you will lock a 1064 nm diode laser to one beam direction of a four mirror ring cavity using the Pound-Drever-Hall (PDH) locking technique. You will analyze the cavity properties and its finesse via the cavity ring-down technique. The cavity sits on a rotating table, which rotation speed can be read off digitally. Locking a second laser beam to the opposite beam direction of the cavity with an acousto-optical modulator, the setup is transformed into a Sagnac laser gyroscope. This will allow you to identify a frequency offset between the two laser beams - the Sagnac frequency - by recording both the optical beat signal of the two beams, as well as by reading of the radio frequency of the locking electronics. With the setup in operation you will analyze its performance and sensitivity by measuring both the scale factor as well as the Allan deviation of the laser gyroscope. If you have time you can attempt a measurement of the rotation rate of Earth.

3 Background information

3.1 Prelude: The rotation of Earth

In the scientific history of mankind, the development of calendars and observatories to keep track of the passing of time is certainly among the earliest achievements. Notable realizations include the famous Maya calendar, as well as the ancient Egyptian and Roman calendars. While many of these have been developed independently from one another, they all build on a measurement of the rotation period of Earth (one day), its orbital period around the Sun (one year), or the orbit of Moon around Earth (one month) with ever increasing accuracy. Here, we will focus on the rotation of Earth, which has traditionally been measured through observation of the apparent movement of the fixed star sky. The ancient Maya people for instance were able to measure and predict the length of a year with a relative uncertainty at the level of 10^{-5} . Their level of instrumentation, understanding, and mathematical competence exceeded the one of the Spanish conquerors of the 16th century.

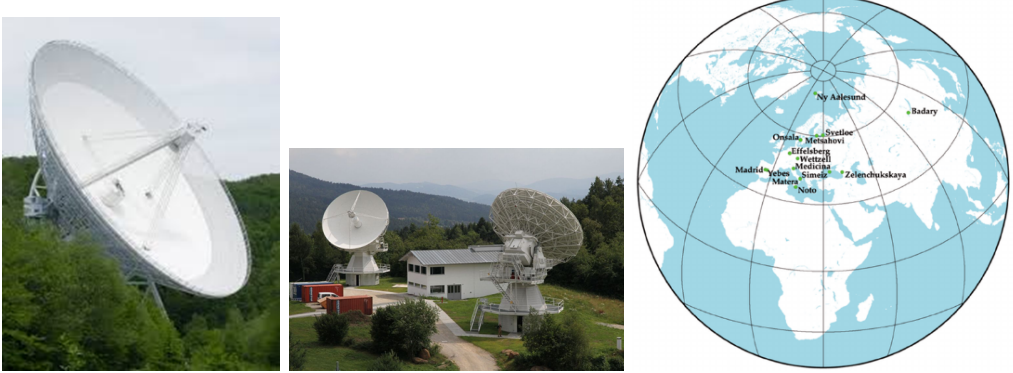


Figure 1: A set of radio telescopes, such as the 100-meter telescope in Effelsberg (left) and the Twin Telescope at the Fundamentalstation Wettzell (center), are connected to form a virtual telescope with much larger effective aperture and redundancy. The stations shown on the right contribute to the European VLBI network.

VLBI and the determination of Earth rotation parameters Today, measurements of various astronomical observatories around the world are combined via very-long baseline interferometry (VLBI), see Figure 1, to yield an uncertainty of a few $10\ \mu\text{s}$ for the length of a sidereal day¹ (fractional uncertainty of a few parts in 10^{-10}). Together with data from the Global Navigation Satellite Systems (GNSS), the three Earth Rotation Parameters (ERPs) are obtained: these include the length-of-day (LoD), as well as the two coordinates of the Earth's rotation axis. The International Earth Rotation Service (IERS) compiles and publishes this data, see Figure 2. Oftentimes, only the difference of the present ERPs from a certain long-term average is of interest, stated as excess LoD (LoD) and as polar motion (PM, x and y). The uncertainty in the daily values of LoD is about $10\ \mu\text{s}$, and the uncertainties in x and y are about $4\ \text{mm}$.

In this way, many fascinating phenomena were observed, such as the increase the rotation period by tidal breaking, the seasonal variations induced by angular momentum exchange with the atmosphere, and a 433-day periodic movement of the Earth's rotation axis known as the Chandler wobble; see Figure 3. The rotation rate of Earth is about $72.92\ \mu\text{rad s}^{-1}$ along its rotation axis, the very-long-term decrease amounts to about 0.01 to $1\ \text{frad s}^{-1}$, and the yearly, monthly, daily, and sub-daily variations are on the scale of 0.01 to $1\ \text{prad s}^{-1}$.

VLBI network are usually not operated continuously: in standard operation, the radio telescopes of a network are linked only twice a week for a few hours to determine the ERPs through observation of a large ensemble of distant radio sources. As a consequence, VLBI shows poor temporal resolution, with a “high-frequency” cutoff corresponding to a few days. The interesting short-term phenomena, among them periodic events such as the tides, and single events such as Earthquakes, can hardly be resolved.

¹The day defined by Earth's orientation relative to fixed stars.

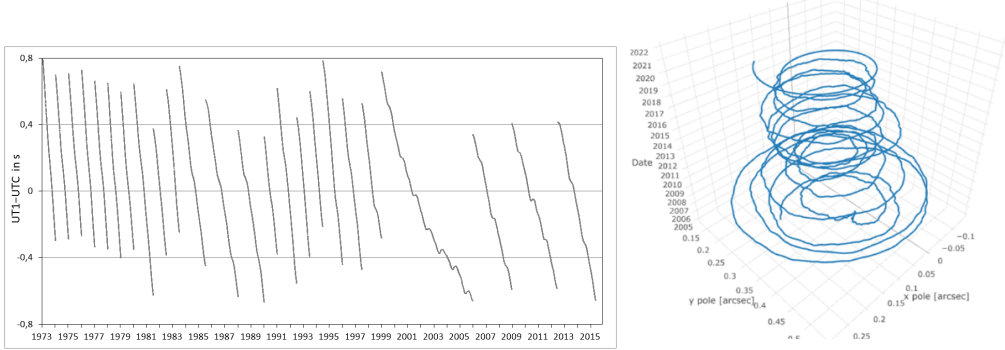


Figure 2: The International Earth Rotation and Reference Systems Service (IERS) publishes the three Earth Rotation Parameters (EPRs): the length-of-day (LoD, left) and the two coordinates of the Earths polar motion (PM, right). Plots taken from www.iers.org.

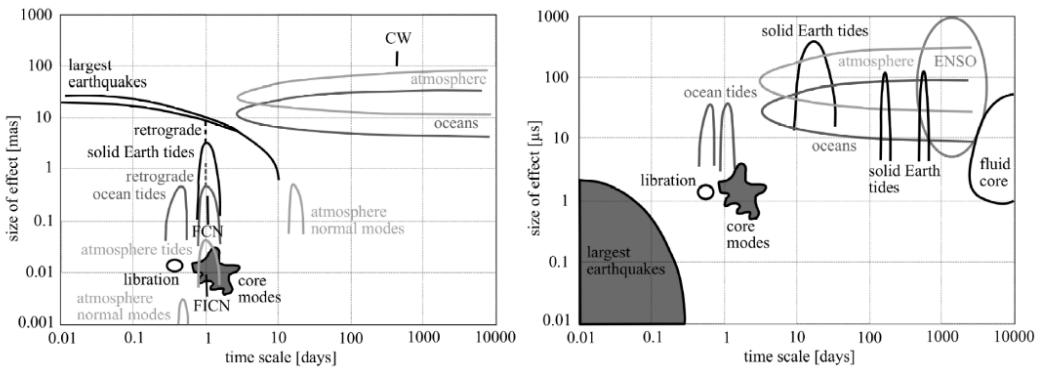


Figure 3: Excitations of polar motion (PM, left) and length-of-day given as variations to the UT1 (LoD, right). Taken from [1], original from <ftp://gemini.gsfc.nasa.gov/pub/core/>.

Climate change effecting the rotation of Earth As the total angular momentum is preserved, large-scale transport of matter, such as postglacial isostatic adjustment, sea level rise, and the melting of ice caps and glaciers, all lead to a change in the rotation period. With increased precision, minuscule changes in the Earths rotation frequency related to climate change can be observed. To give an estimate, the melting of polar ice caps currently leads to an average global sea level rise of $3.1(4) \text{ mm yr}^{-1}$ (2.0 mm yr^{-1} of which are mass-related), which increases the length-of-day by $1.2 \mu\text{s}$ per year. Observing these very slow developments puts stringent requirements to the long-term stability of any observation.

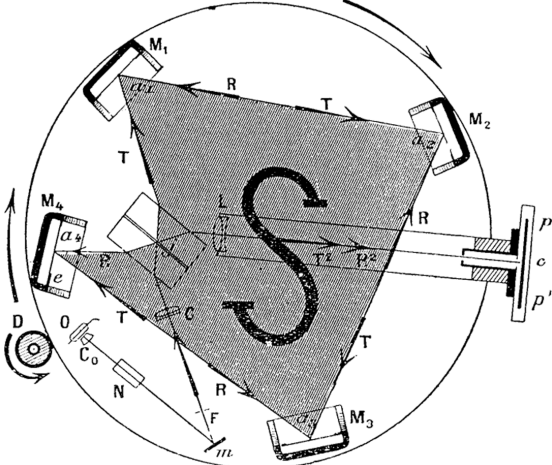


Figure 4: George Sagnac (left) and his interferometer setup (right).

3.2 Gyroscopes based on the Sagnac effect

3.2.1 The Sagnac effect

Consider a circular light path of perimeter P that encloses an area A and two contra-propagating light fields of the same wavelength λ propagating along this trajectory, e.g. one clockwise and one counter-clockwise beam. When overlapped behind a beamsplitter, these two beams will form a stable interference pattern. Now the arrangement is set in rotation; therefore the effective optical paths lengths of the two beams, required for one roundtrip, changes. The effective path of the co-rotating light field is stretched, while the path of the counter-rotating light field is contracted. The resulting phase shift

$$\delta\phi = \frac{8\pi A\Omega}{c\lambda} \quad (1)$$

is proportional to the projection of the enclosed area vector onto the rotation vector. This phase shift was first measured by George Sagnac (1869 - 1926) through a shift at the output of an interferometer, the design of this setup is reprinted in Figure 4.

We will pause here for a brief statement: For translations, Einstein theorem tells us that it is in principle not possible to tell whether one's inertial system is moving or not. The analogous statement for rotations is false! It is indeed possible (with only a simple light source, a set of mirrors, and a detector!) to measure the rotation rate of one's inertial system. Thus, translation and rotation are fundamentally different concepts.

Derivation of the Sagnac effect The notion of the Sagnac effect is rather intuitive and can be described in plain arguments such as “the mirrors are moving away from the light” and “the mirrors are moving towards the light” in connection with the constancy of the speed of light. Yet, the Sagnac effect is a direct consequence of the theory of relativity, see Reference [5] for a derivation.

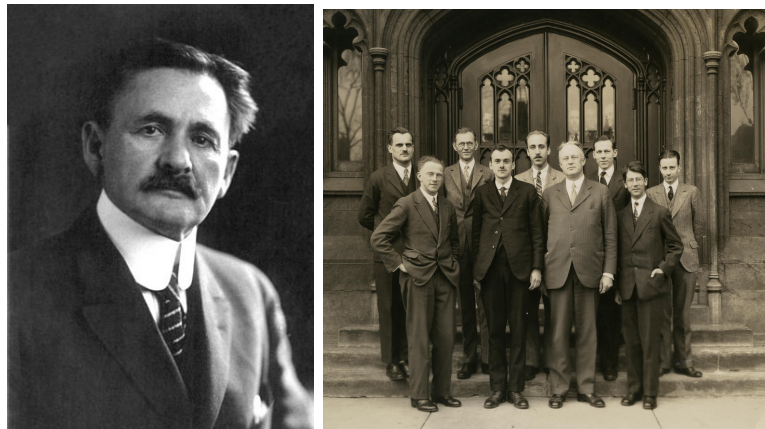


Figure 5: Left: Albert A. Michelson (1852 – 1931) performed a number of experiments to measure the speed of light and to prove or disprove the existence of an ether. Right: Henry Gale, an astronomer in Chicago, (1874 – 1942; front row, third person from the left) right next to some of the founding fathers of quantum mechanics. Can you spot Werner Heisenberg, Paul Dirac, and Friedrich Hund?

3.2.2 Early gyroscopes: the Michelson-Gale experiment

Albert A. Michelson was a Nobel laureate well known for his work on the interferometer that is today known by his name. While he also devoted much of his scientific work to an ever more precise measurement of the speed of light, he also set up the first large-scale gyroscope to measure the rotation rate of Earth itself. The first proposal was phrased as early as 1904: the two arms of a standard Michelson-Morley interferometer were to be replaced by two rectangular beam paths, a small one and a very large one. First experimental attempts were operated in air and failed due to turbulences and attenuation that deteriorated the fringe contrast.

Albert A. Michelson then teamed up with Henry Gale for a new attempt. A sufficiently large piece of land in the Chicago area was secured, and a sewage company was convinced to evacuate more than 2 km of piping. The design of the experiment is shown in Figure 6: The (incoherent) light emission of a carbon arc is spectrally filtered, collimated, and sent through a beamsplitter. The interferometer is closed through two contra-propagating beam paths with a length of about 650 m, which however enclose only a negligible area. By flipping two mirrors, the area can be increased drastically to about 0.2 km^2 . The rotation of Earth then induces, through the Sagnac effect, an expected relative shift in the fringe pattern by 0.237 fringes. The experiment revealed a shift of $0.230(5)$ fringe periods. What an astonishing agreement between the experiment and the simple theoretical expectation.

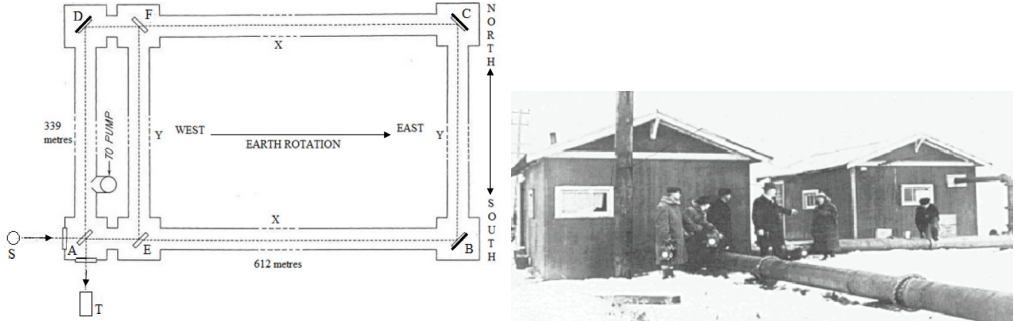


Figure 6: Top: Layout of the Michelson-Gale-experiment. A glowing carbon filament is used as an (incoherent) light source (S), the light is split up into two pathways at the beamsplitter A. Depending on the orientation of mirrors E and F, the Sagnac ring is formed by mirrors A, E, F, and D (negligible enclosed area) or by mirrors A, B, C, and D (0.2 km^2 enclosed area). Bottom: A photograph of the setup. The source and detector, as well as mirrors A and E, are located in the shed to the left. The right shed houses the vacuum pumps.

3.2.3 Active ring laser gyroscopes

So far, we have considered a beam of light split into two arms of an interferometer to measure a phase shift. Now, we will advance from phase shift measurement to a frequency measurement. To this end, we allow two contra-propagating longitudinal modes of a ring cavity to have different frequencies. The ring cavity would usually be of a triangular or square shape. Light of both modes that leaks through one of the mirrors can be interfered on a beamsplitter, and the observed beat frequency $\delta\nu$ is just the Sagnac frequency proportional to projection of the rotation vector $\vec{\Omega}$ onto the vector of the enclosed area \vec{A} :

$$\delta\nu = \frac{4\vec{A} \cdot \vec{\Omega}}{\lambda P} \quad (2)$$

For now, we will consider only square ring cavities with four arms of length L ($A = L^2$, $P = 4L$) that are oriented normal to the rotation vector ($\vec{A} \parallel \vec{\Omega}$). The expression for the Sagnac frequency then simplifies to

$$\delta\nu = \frac{L\Omega}{\lambda} \quad (3)$$

In other words, the Sagnac frequency is n times the rotation rate, where $n = L/\lambda$ is the number of nodes of the light field in each arm.

The sensitivity of such a ring laser gyroscope will depend on the arm length L of the gyroscope, the wavelength λ used, and the finesse F of the ring resonator². A photodetector is used to measure the beat signal and we will assume photon shot-noise limited detection, where $N = P_{\text{opt}}/(h\nu)$ photons reach the detector per unit time, with

²For the latter see Section 3.3.2.

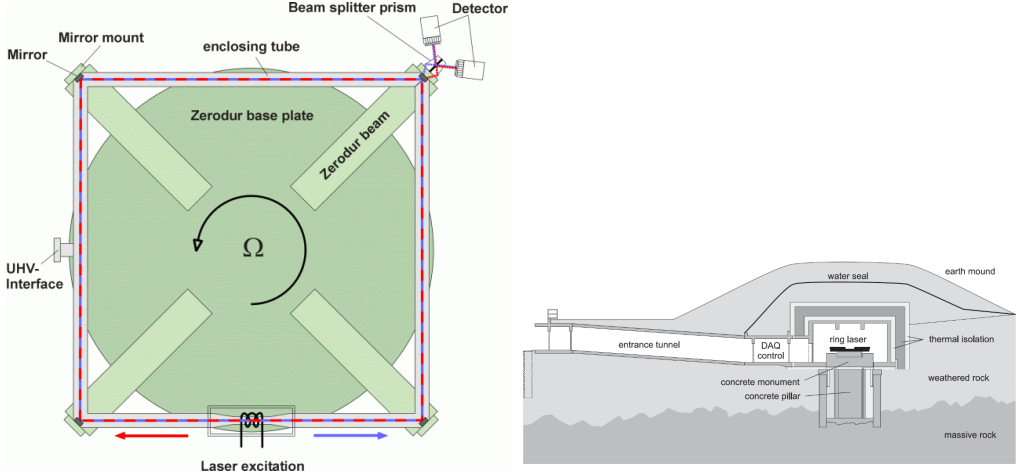


Figure 7: The G-ring at Wettzell. Left: Experimental layout, showing the $4 \times 4 \text{ m}^2$ Sagnac ring with the laser medium in the bottom tube and the interferometer used for detection in the top right corner. Right: The ring is mounted horizontally, on a massive foundation cast onto bedrock to rigidly connect to the rotating Earth. The site is covered by a few meters of overburden for thermal insulation.

P_{opt} being the optical power available for the measurement. Then, for an integration time τ the gyroscope's sensitivity to a rotation rate Ω is given by

$$\delta\Omega = \frac{1}{4} \frac{c\lambda}{L^2 F} \sqrt{\frac{h\nu}{P_{\text{opt}}}} \frac{1}{\tau} \quad (4)$$

The best usable sensitivity reported thus far is reached by the G-ring at the German Fundamentalstation Wettzell with about $12 \text{ prad/s}/\sqrt{\text{Hz}}$. This device is an extremely stable so-called active ring laser gyroscope and shall be described in the following.

The G-ring features four mirrors with very high reflectivity (losses of only a few ppm), mounted onto a quasi-monolithic Zerodur structure³, to form a cavity with a finesse of 138 000 and an arm length of 4 m [2]. The arms are set under vacuum, and a section of the ring is filled with a helium/neon gas mixture. This gas is excited through a radio frequency and starts lasing on the modes of the ring cavity near 633 nm. The free spectral range of this comparably large cavity is rather small, only 18.75 MHz, which is smaller than the gain width of the HeNe gas. Consequently, the medium lases on a multitude of longitudinal modes and takes a long time to settle into stable operation. Single-mode operation can be enforced by operation very close to the lasing threshold, but then only a few 10 nW of power are emitted through the mirrors and are available for detection.

The device is mounted horizontally and thus senses Earth's rotation. The co- and counter-rotating modes are non-degenerate and split by the Sagnac frequency of 47.6 kHz

³A glass ceramic with a thermal expansion coefficient $\alpha < 1 \times 10^{-8}$

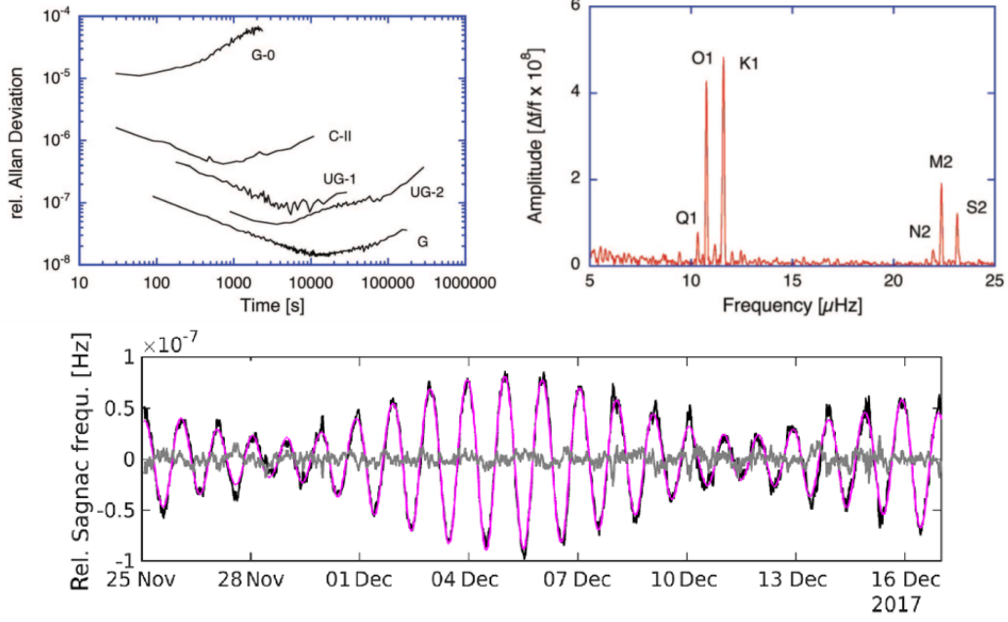


Figure 8: Performance of the G-ring at Wettzell. Top left: Allan deviation of various ring laser gyroscopes. The G-ring (G) reaches a relative instability of about 1×10^{-8} after three hours of integration, which would correspond to 1 ms variations in LoD. Top right: A Fourier spectrum of the measurements, using about half a year of data. Signals at frequencies of about one day (denoted as K1) and half a day (S2), related to the tides, are clearly visible. Bottom: A comparison between VLBI data (magenta) and gyroscope data (black) for an extended measurement campaign of about three weeks. The difference signal is plotted in grey and shows agreement well below the 1×10^{-8} level. The diurnal oscillations in the Earth's rotation rate are clearly visible, just as a 14-day modulation of its amplitude.

(the latitude of Wettzell is about 49.1° north). This frequency is monitored continuously. The high stability of the device allows for long periods of data acquisition; see Figure 8. A sensitivity of $12 \text{ prad/s}/\sqrt{\text{Hz}}$, integrated over 3 h ($\approx 1 \times 10^4 \text{ s}$), yields an uncertainty of 0.12 prad s^{-1} in the Sagnac frequency. At this relative uncertainty the larger variations in the Earth rotation rate come into reach.

After many hours, temperature changes on the laboratory lead to a length change of the cavity, and small changes in the tilt of the gyroscope, already stabilized at the μm -level, change the projection onto the Earth rotation axis. Still, the sensitivity of the G-ring is sufficient to measure both long-term phenomena such as the Chandler-wobble [2], as well as the diurnal and sub-diurnal variations of Earth rotation, see Figure 8. Comparison with continuous VLBI data, taken over a period of many days, shows excellent agreement.

3.2.4 Passive ring laser gyroscopes

The so-called active ring lasers presented in the proceeding section have the lasing medium located directly inside the resonator. This ensures intrinsically very narrow linewidths, but the lasing medium can also induce systematic uncertainties. An alternative design would be the so-called passive ring laser, where an external laser is locked to the two counterpropagating modes of the resonator. The sensitivity of any ring laser, both active and passive, is given in Equation (4). For a given geometry (wavelength, size, and mirror quality, reflected in the finesse), the light intensity available for detection is the only free parameter. Here, active ring lasers need to be operated just slightly above the lasing threshold to reduce mode competition (recall that the gain width is larger than the free spectral range), which limits the available light power to a few 10 nW. On the other hand, passive ring lasers can be operated at substantially higher powers (recall that the gravitational wave detectors inject MW-levels of power into the interferometer arms). Removing the lasing medium from within the sensor reduces systematic errors, but adds the complexity of analog and digital electronic for laser locking.

Two state-of-the-art passive ring laser gyroscopes are described in References [3] and [4]. These two realizations are geared towards rotation sensors for the mirror stations of next-generation gravitational wave detectors, but could also be employed for geodetic observations. The device used for this lab course is a down-scaled and simplified version of these two experiments. In order to increase the Sagnac frequency from a few 10 Hz, as induced by Earth's rotation, to the 10s of kHz regime, our gyroscope is mounted on a rotating table.

3.3 Fundamentals of optical cavities

The core of any free-space laser gyroscope is its cavity. Different to standard optical cavities, so called Fabry-Pérot interferometers [7], the here considered resonator consists of four instead of two spherical mirrors. It is however very easy to transfer the description of cavity properties from the two-mirror cavity to our ring resonator.

3.3.1 Cavity modes

For any optical resonator made out of parabolic mirrors and an optically homogenous medium, the coherent electric field inside cavity can be decomposed into Hermite-Gaussian modes, which are solutions to the paraxial Helmholtz equation when considering the decomposition into Cartesian coordinates x and y orthogonal to the beam propagation direction z [7].⁴ In the cavity, the propagating beam's wavefront matches the radii of curvature of the mirrors radii, see Figure 9.

The Hermite-Gaussian modes are also called transversal electro-magnetic modes and are labeled by $\text{TEM}_{m,n}$, where $m, n \in \mathbb{N}^{\geq 0}$ are integers associated to the order of the Hermite-polynomials along the x and y direction. Their resonance frequencies are given

⁴Note that spherical symmetric resonators are mostly better described by the orthogonal set of Laguerre-Gaussian modes, an alternative basis.

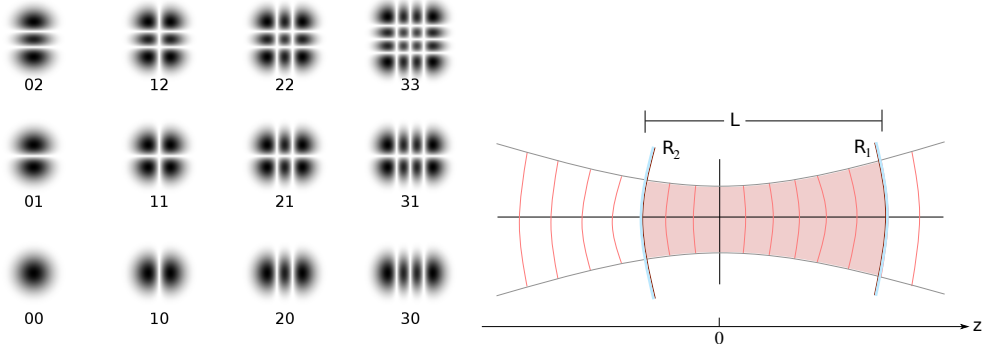


Figure 9: Hermite-Gaussian transverse electro-magnetic mode $\text{TEM}_{l,m}$ patterns (left) and the beam's wavefront inside a cavity defined by two mirrors with radii R_1 and R_2 respectively (right).

by

$$\nu_{l,m,n} = \delta\nu_{\text{FSR}} \left(l + (m+n+1) \frac{\delta\zeta}{\pi} \right), \quad (5)$$

where $l \in \mathbb{N}^{\geq 0}$ is an integer denoting the different transversal resonances (= longitudinal nodes). $\delta\nu_{\text{FSR}}$ is the free spectral range, the spacing of the longitudinal modes, given by the perimeter P of the cavity via:

$$\delta\nu_{\text{FSR}} = \frac{c}{P} \quad (6)$$

The Hermite-Gaussian field accumulates a phase difference of $\delta\zeta = \zeta(P) - \zeta(0)$ per roundtrip, where $\zeta(z) = \arctan(z/z_R)$ is the Gouy phase with $z_R = \pi w_0^2/\lambda$ the Rayleigh length and w_0 the minimum beam waist radius. This determines the transversal mode spacing.

The ground mode is the $\text{TEM}_{0,0}$ Gaussian beam, that is the preferred mode for locking our laser beams. The shape of higher order transversal modes differ from a two-dimensional Gaussian due to the corresponding Hermite polynomials, see Figure 9. Knowing the precise location of the higher order transversal and longitudinal modes is crucial, when designing a cavity and choosing its perimeter, since competition of neighboring modes can for instance lead to unstable laser locks.

Also important when designing a cavity: A two-mirror resonator can support any mode if the two mirror radii R_1 and R_2 fulfill the stability condition

$$0 \leq g_1 g_2 = \left(1 - \frac{L}{R_1}\right) \left(1 - \frac{L}{R_2}\right) \leq 1 \quad (7)$$

For a four-mirror ring cavity $g_1 g_2$ and the adapted condition can be generally computed as the magnitude of the eigenvalues of the ABCD transfer matrix for a roundtrip.

Airy lineshape and optical cavity ringing When scanning the laser frequency of a coupled mode the power transmitted through the cavity mirrors is expected to follow the Airy function, a Lorentzian like lineshape. “While this is true for small scanning speeds and cavities with relatively low finesse, one can observe an asymmetrical response and a deformation of the Airy peak, similar to a ringing, for high finesse cavities. This effect arises, when the laser is swept over the optical resonance in a time shorter than the cavity storage time. If this condition is fulfilled the cavity does not have enough time to fill itself as the resonance is approached. The evolving field inside the cavity and the incoming field start to beat and give rise to the oscillatory behavior.”[8] This effect will be visible in all cavity signals that we will look at in the course of this lab experiment.

3.3.2 Finesse

The finesse is the main quality characteristic of any cavity and determines its spectral linewidth $\delta\nu_{1/2}$, the full width half maximum (FWHM) of the transmission peaks. Here a high finesse equals a narrow resonance line, which is required for high precision frequency applications. It strongly depends on the mirror reflectivities but is independent of the resonator length and can be written as

$$\mathcal{F} = \frac{\delta\nu_{\text{FSR}}}{\delta\nu_{1/2}} \approx \frac{\pi\sqrt{\mathcal{R}}}{1 - \mathcal{R}} \quad (8)$$

where $\mathcal{R} = \sqrt{\mathcal{R}_1\mathcal{R}_2\mathcal{R}_3\mathcal{R}_4}$ describes the reflectivity \mathcal{R}_i of the cavity mirrors and the approximation holds true for high reflectivities (= low losses) $(1 - \mathcal{R}) \approx 0$, which is generally the case when dealing with finesse quantification.

Cavity-ring-down technique Mirror reflectivities itself are hard to measure precisely. To experimentally measure the finesse of a cavity we can look at the temporal evolution of the optical power in the cavity, when switching off the cavity-locked laser rapidly. This can for instance be done by quickly switching the RF signal driving an acousto-optical modulator (AOM).

Neglecting the losses in the cavity medium – a good assumption for infrared light in air – starting with an initial laser intensity I_0 every roundtrip in the cavity will reduce the circulating power by a factor \mathcal{R}^2 . Therefore when switching off the laser light at time $t = 0$, the time evolution of the laser intensity for $t \geq 0$ is given by

$$I(t) = I_0 \mathcal{R}^{2t/\tau_r} = I_0 \exp\left(-\frac{t}{\tau_{\text{dec}}}\right) \quad (9)$$

where $\tau_r = P/c$ is the roundtrip time and the decay time τ_{dec} is given by

$$\tau_{\text{dec}} = -\frac{\tau_r}{\log \mathcal{R}^2} = -\frac{P}{c \log \mathcal{R}^2} \quad (10)$$

3.3.3 Pound-Drever-Hall locking

Pound-Drever-Hall (PDH) locking is a very common and powerful tool to frequency stabilization a laser to any optical reference, spectroscopy and cavity stabilization are the most widespread applications. Beyond optical applications, PDH locking can also be found in many other fields and applications. The following introduction to PDH laser frequency stabilization is extracted from Reference [6]; more technical details can be found in the application note of the laser lock box manufacturer, see Reference [9].

In the case of PDH stabilization to an optical cavity, like a Fabry-Pérot or our ring resonator, the cavity back-reflection of a frequency modulated light field is recorded by a photodiode and fed into a closed control loop, most often a proportional-integral-differential (PID) controller, that talks back to the laser.

The incoming light field E_{in} oscillating at ω and modulated by a frequency Ω – in most cases created by means of an electro-optical modulator – can be, in first order, approximated as sum of three frequency components:

$$E_{\text{in}} = E_0 e^{i(\omega t + \beta \sin(\Omega t))} \approx E_0 \left(J_0(\beta) e^{i\omega t} + J_1(\beta) e^{i(\omega+\Omega)t} - J_1(\beta) e^{i(\omega-\Omega)t} \right) \quad (11)$$

where J_k are the Bessel functions and β is the modulation depth. This is a good approximation for small modulation depths $\beta < 1$, the total laser power then splits nearly completely into the carrier $P_c = J_0^2(\beta) |E_0|^2$ and sidebands $P_s = J_1^2(\beta) |E_0|^2$, such that $P_0 = |E_0|^2 \approx P_c + 2P_s$. [6]

The light field frequency components are then reflected according to the complex frequency dependent reflection coefficient $F(\omega) = E_{\text{ref}}/E_{\text{in}}$, resulting in a three dip structure when scanning the laser over the resonance, see Figure 10. The signal is recorded with a fast photodiode (frequency bandwidth $\gg \Omega$) and the resulting RF signal, that contains terms at frequency $\pm\Omega$ as well as 2Ω , is demodulated at the local oscillator frequency Ω using a RF mixer. Subsequent low pass filtering removes higher frequency components (e.g. terms oscillating at 2Ω) and leads to DC error signal that samples the phase of the reflected carrier, see Figure 10. This error signal shows (after offset correction) a zero crossing and a steep linear slope around the cavity resonance, that is then fed back via the PID control loop for stabilizing the laser. The slope of the error signal depends on the distribution of carrier and sideband power, as well as the cavity linewidth $\delta\nu_{1/2}$ [6]:

$$\epsilon \propto -\frac{4}{\pi} \sqrt{P_c P_s} / \delta\nu_{1/2} \quad (12)$$

When selecting good PID parameters for correcting both fast as well as slow laser lock disturbances, this technique therefore allows frequency stabilization to a fraction of the cavity linewidth; world class cavities with ULE spacers reaching sub mHz laser linewidths. The theoretically optimal power ratio between the carrier and sideband to reach the steepest PDH error signal is achieved at a modulation depth of $\beta = 1.08$ which is equivalent to a relative first-order sideband height/power of 42 % compared to the carrier. For proper demodulation of the photodiode signal furthermore the relative phase of the frequency components at Ω between the photodiode signal and the local

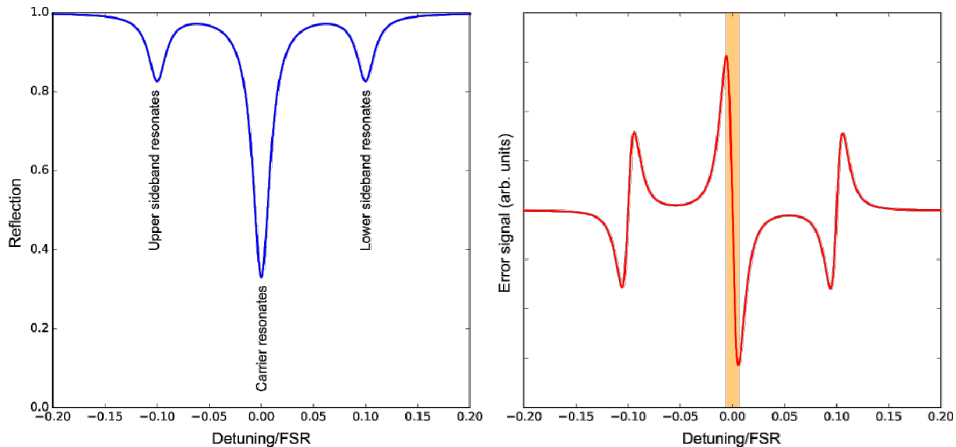


Figure 10: Pound-Drever-Hall (PDH) cavity reflection (left) showing the three frequency components, the carrier ω and two sidebands $\omega \pm \Omega$ when scanning the laser over the cavity resonance ω_0 . Here Ω has to be chosen greater than the linewidth of the cavity to separate the peaks. The resulting error signal after frequency demodulation (right) shows a steep linear slope around the cavity resonance, that can be used for PID feedback to stabilize the laser. The x-axis shows the laser detuning $\Delta = \omega - \omega_0$. Figures are taken from Reference [9].

oscillator port of the frequency mixer is very important and also determines the sign of the error signals slope.

Residual amplitude modulation “No electro-optic phase modulator is perfect and there will always be a small residual amplitude modulation (RAM) of the laser beam [11]. This effect can be further increased if the beam polarization does not perfectly align with the polarization axis of the EOM crystal. In this case, the output beam’s polarization will exhibit an oscillatory rotation and every polarization-sensitive optical element will translate this directly into amplitude modulation. Any RAM will disturb the PDH locking scheme by introducing a frequency offset. As long as the RAM is constant, the offset is also constant and can be corrected, but RAM fluctuation due to temperature noise is unavoidable and can be a major source of frequency stability degradation.” [8]

3.3.4 The lock-in effect

The so-called lock-in effect is ubiquitous in physics: two oscillators with slightly different frequencies will synchronize (“lock” to exactly the same frequency) if there is a weak coupling between them. The most prominent example is the one of two pendulum clocks hung upon the same wooden wall: if their individual resonance frequencies are sufficiently close, they will synchronize and tick in unison. The range over which these two clocks actually synchronize depends on the coupling strength between the two pendula, and the unperturbed frequency difference f_0 . In general, the frequency difference between

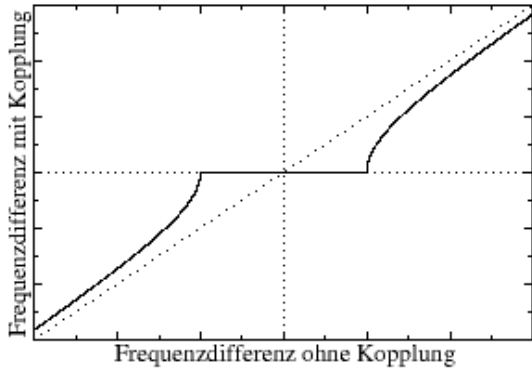


Figure 11: The lock-in effect. Below a certain threshold, the frequency difference between two oscillators is zero. Above this threshold, the coupled frequency difference approached the uncoupled frequency difference. Figure taken from <https://www.uni-potsdam.de/u/physik/fprakti/moderne-themen/Hannig-Synchronisation%20von%20Pendeluhren%20und%20Metronomen.pdf>

the two pendula is

$$\delta f = \sqrt{f_0^2 - f_L^2}, \quad (13)$$

where f_L is the lock-in threshold, below which the two pendula synchronize; see Figure 11. This lock-in effect is also found in RF electronics and optics.

In the case of gyroscopes, the two oscillators are the two counter-propagating longitudinal modes of the ring cavity. The coupling between these two modes is provided by backscattering of the mirrors. The scattering losses of our mirrors (ion-beam sputtered coating at 1064 nm) is only a few ppm, but can increase substantially through deposition of dirt. For comparison, the absorption losses are a few ppm, and transmission is about 10 ppm. The light is scattered into the solid angle, and a very small fraction is coupled into the counter-propagating mode, thereby transferring energy from one mode to the other. The lock-in threshold is estimated as

$$\Omega_L = \frac{c\lambda^2 r_s}{32\pi Ad}, \quad (14)$$

where λ is the laser wavelength, A the enclosed area of the cavity, d the cavity modes beam diameter and r_s the fraction of backscattering as compared to all other losses [2]. We estimate the value of r_s to have an upper limit of about $r_s^2 \lesssim 4(1 - R) = 4(1 - \sqrt{R})$.

With the present setup, the lock-in threshold is much larger than the Earth rotation rate of about $55 \mu\text{rad s}^{-1}$. This will limit us strongly in trying to observe the Earth rotation rate. A larger ring and reduced scattering losses would be required to reduce the lock-in threshold. The first ring laser gyroscope to unlock and measure the Earth rotation rate was the C-ring at Canterbury (Australia) in 1990, with an area of 1 m^2 and an operating wavelength of 633 nm.

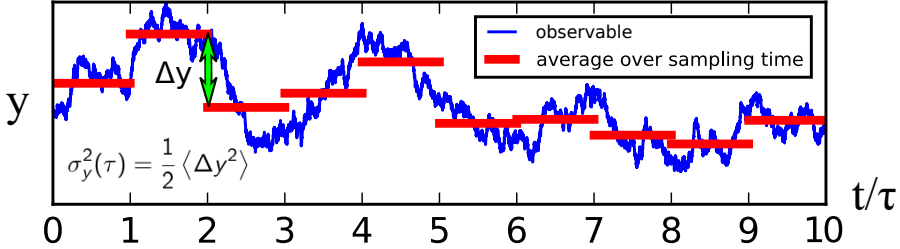


Figure 12: Temporal fluctuations of an arbitrary observable y , from which the time averages (indicated by the red bars) for a given integration time τ are taken. The Allan deviation for a specific averaging time is defined as half the mean value of the difference between consecutive temporal averages squared.

3.4 Quantifying performance: the Allan deviation

Now, how do we quantify the performance of a gyroscope? Or, more generally, how can the instability of any device be specified? Here, we will introduce the Allan deviation as a measure of stability.

Consider two almost identical devices that measure the same frequency. Typical examples could be two optical clocks that interrogate the same optical transition, or two gyroscopes that measure the rotation of a common object. We will assume the simplest case of a purely shot-noise limited measurement, which means: the precision increases with the square root of the number of photons we have available for detection, with the square root of the measurement time and with the square root of the oscillators we can interrogate. Also, we assume dead-time free interrogation, limitation through quantum projection noise, and various other simplifications. Then, the measurement sensitivity of the quantity y depends on the measurement time τ as

$$\sigma_{\text{ad}}^2(\tau) = \frac{1}{2M} \sum_{n=1}^M (\bar{y}(\tau)_{n+1} - \bar{y}(\tau)_n)^2 \quad (15)$$

where M is the number of samples and $\bar{y}(\tau)$ is the temporal average of the observable y over the time τ .

The value σ_{ad} is called the Allan deviation (the square σ_{ad}^2 is known as the Allan variance) and is usually plotted on a log-log diagram versus the time intervals τ . The basis of such a plot is formed by a sufficiently large set of measurement data (e.g. frequencies or frequency differences) obtained at regular time intervals. Then, the value of τ is varied from the smallest increment up to half the total measurement time T . For each value of τ , the averaged values $\bar{y}(\tau)$ are calculated to give the sum of Equation (15). Most software tools (`python`, `Mathematica`, ...) provide built-in functions to calculate the Allan deviation, often named `ADEV`. Usually, slightly advanced versions such as the overlapping Allan deviation (`OADEV`) or more generally, modified Allen deviations (`MADEV`) are used.

For the typical shot-noise scaling $\propto 1/\sqrt{\tau}$, also referred to as random walk, the curve

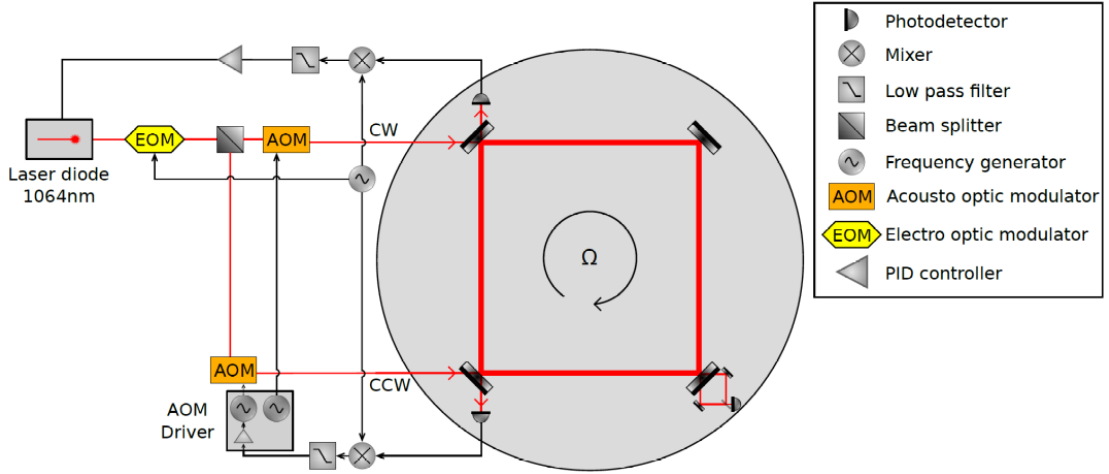


Figure 13: Setup of the experiment. Figure taken from C. Wind master thesis [8].

has a slope of -0.5 , here

$$\sigma_{\text{ad}}(\tau) = \frac{\mathcal{A}}{\sqrt{\tau}} \quad (16)$$

The parameter \mathcal{A} is often given to quantify the shot-noise limited sensitivity.

The Allan deviation serves as a probe to determine whether the sensitivity of the measurement device really shows the expected shot-noise, and how long this scaling can be maintained. For any technological device, systematic effects will lead to drifts (bias instabilities) at some point, which will eventually become larger than the stability obtained through statistics. Such drifts can be induced by deformations of the measurement device through ageing or temperature drifts, ageing of electronics, local movements, and so on. The only question is: how stable is the measurement device, that is: how long can we measure until the drifts exceed the stability? At this point, the Allan deviation (on a log-log plot) deviates from the linear -0.5 slope, it levels off and starts to increase again; see Figure 8 for an example. The minimum value reached in the Allan deviation is referred to as the instability of the measurement device, often given as a relative instability. The very best ring laser gyroscopes reach relative instabilities in the 1×10^{-8} range, limited by residual tilt and temperature/air pressure fluctuations. Optical clocks can even reach relative instabilities in the 1×10^{-19} range.

4 The setup

A interference filter diode laser in cat-eye configuration (Moglabs CEL) at $\lambda = 1064$ nm is used as the light source. Its light is coupled into a fiber and then sent into a fiber-based electro-optical phase modulator (EOM), where the PDH sidebands at a frequency of $\Omega/(2\pi) = 10$ MHz are applied. The two light beams are coupled out of the fiber and split into two beams of equal power, each of which is sent through an acousto-optical

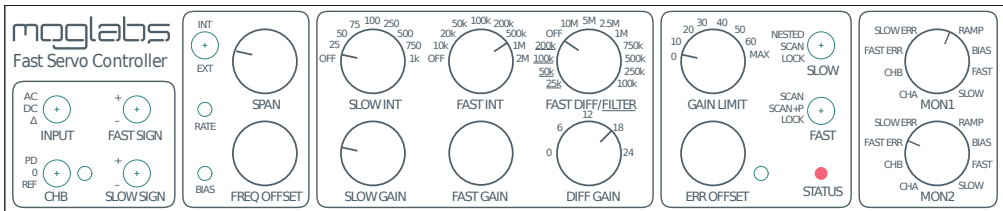
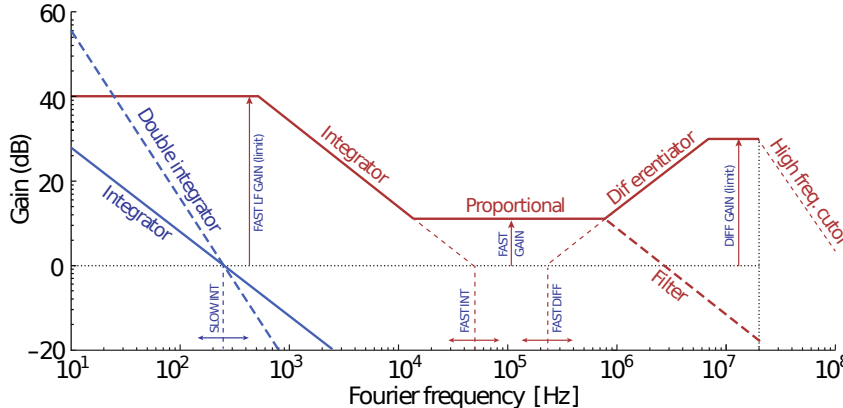


Figure 14: Moglabs FSC fast servo laser lock box. Pictures are taken from the manufacturers manual, see Reference [10].

modulator (AOM) at about 200 MHz. The frequency shifted first order diffraction of the AOMs are afterwards again fiber coupled and send through 5 m long, polarization maintaining optical fibers to the gyroscopes cavity. Half waveplates are used to control the light polarization in the cavity since the cavity mirror reflectivity is strongly dependent on it.

The heart of the experiment is formed by a square cavity with an arm length of about 25 cm that is sitting on a rotatable table.⁵ It consists of four highly reflective mirrors, one of which is curved with a radius of curvature of -1.5 m and the others being planar. Two laser beams can be coupled into the resonator: one clockwise and one counter-clockwise mode. These two beams enter the cavity through two different mirrors. Because the mirrors are directly exposed to the laboratory environment, degradation of the mirror's reflectivity through dust is expected. To reduce this effect and passively thermally stabilize the ring cavity, the cavity table is encased in a plexiglass housing.

For locking the two beams to the resonator, the reflection of the two beams are collected from the incoupling mirror and send to two amplified photodiodes, that are also located on the rotating table. They get their power and transmit their signals through 5 m long cables that are tied together with the optical fibers and can be wound up when rotating the optical table a few times.

One of the AOM is sitting at a fixed frequency and the corresponding laser beam and cavity reflection signal is used to lock the master diode laser to the respective cavity mode. For that a fast PID servo controller (Moglabs FSC) takes the mixed down error

⁵The measured cavity perimeter is $P = 99.0(5)\text{ cm}$.

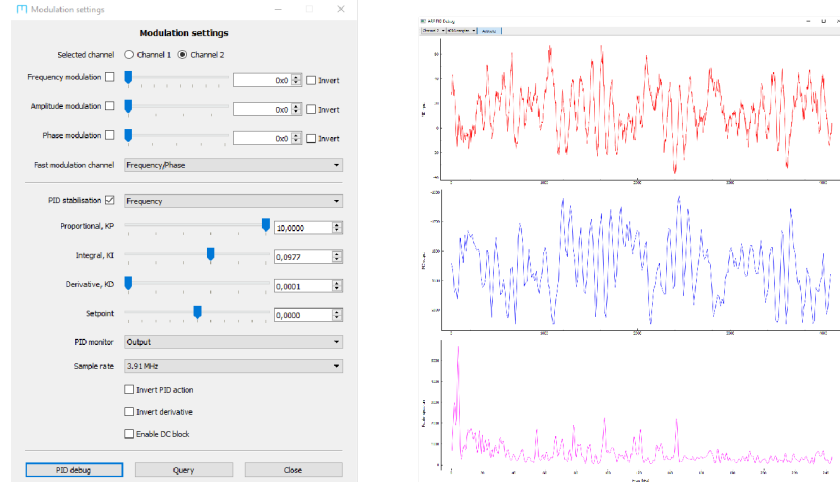


Figure 15: Moglabs AOM driver lock software. “The software allows to directly tune the PID parameters and the error signal setpoint. Additionally, it is possible to invert the PID action which is helpful to correct the feedback sign when necessary. The debug monitor (b) allows for an observation of the PID input and output during the lock and can be used for the optimization of the PID parameters.” Figure and description taken from Reference [8].

signal, applies an offset correction and a PID frequency response and feeds back to the diodes laser controller that controls the laser diodes current (fast) and the interference filter piezo (slow), both of which determine the laser frequency directly. The laser lock is separated in a slow and fast loop, both of which control and respond to different time domains of frequency noise. The control loops frequency response and the laser locks front panel is shown in Figure 14.

The laser lock box also allows to scan the laser controlling both frequency offset and span, which is key in initially finding the cavity resonances (which are located every $\delta\nu_{\text{FSR}}$ in frequency space). For locking one has to zoom into the error signal, such that the resonance zero crossing of the error signal is slightly to the left of the scans frequency offset.

The other cavity reflection is used to lock the second beam to the cavity. To this end, the signal is similarly mixed down with the EOM modulation frequency, lowpass filtered and then sent to the AOM driver control box (Moglabs ARF). This has a built-in PID controller that is managed from a computer software interface as depicted in Figure 15. It allows to steer the AOM frequency and therefore the laser beams frequency around 200 MHz to compensate for the relative frequency difference between the two cavity modes and therefore the Sagnac frequency. For locking the second arm to the cavity the table therefore has to rotated slowly, because otherwise the two cavity modes have no frequency offset.

The light fields transmitted through one of the other cavity mirrors are overlapped on a beamsplitter cube and coupled into a fiber. A photodiode behind the fiber can detect

the frequency difference between these two modes as a beat signal. When blocking one of the cavity modes it can also be used to monitor the cavity transmission for the application of a cavity ring-down measurement. For this, a sufficiently fast photodiode has to be used (and terminated with $50\ \Omega$) to be able to record the fast cavity response (on the order of $10\ \mu s$) when switching off the light using the AOM. The latter is fast enough ($\ll \mu s$) to not limit the measurement by its switching speed.

Another way of measuring the difference frequency of the two cavity modes is the monitor output of the AOM driver, that gives out RF signals in phase with the two AOMs driving frequencies and therefore is also sensitive to frequency differences between the two cavity modes when locked. These two signal can be mixed down using a RF mixer and the resulting signal oscillates therefore oscillates at the Sagnac frequency.

For monitoring, measuring and long-term recording of any signal in the lab a four-channel digital storage oscilloscope (Picoscope) connected to a desktop computer is available.

The rotating table is controlled via a motor; a voltage sets the rotation speed and its polarity the sense of rotation. The rotation rate can be read out via a rotary encoder. The output of the rotary encoder are two TTL signals that switch between high and low depending on the angular position. Each round trip contains 10 000 steps and each step is indicated by a rising or falling edge of either signal. Accordingly each step translates to a rotation of 0.036° . [8]

A photo of the gyroscope lab experiment setup in Figure 16 shows the optical elements on the rotating table, where the laser beam is coupled out of fibers (green) into the gyroscope cavity (red) and the transmission is observed (yellow).

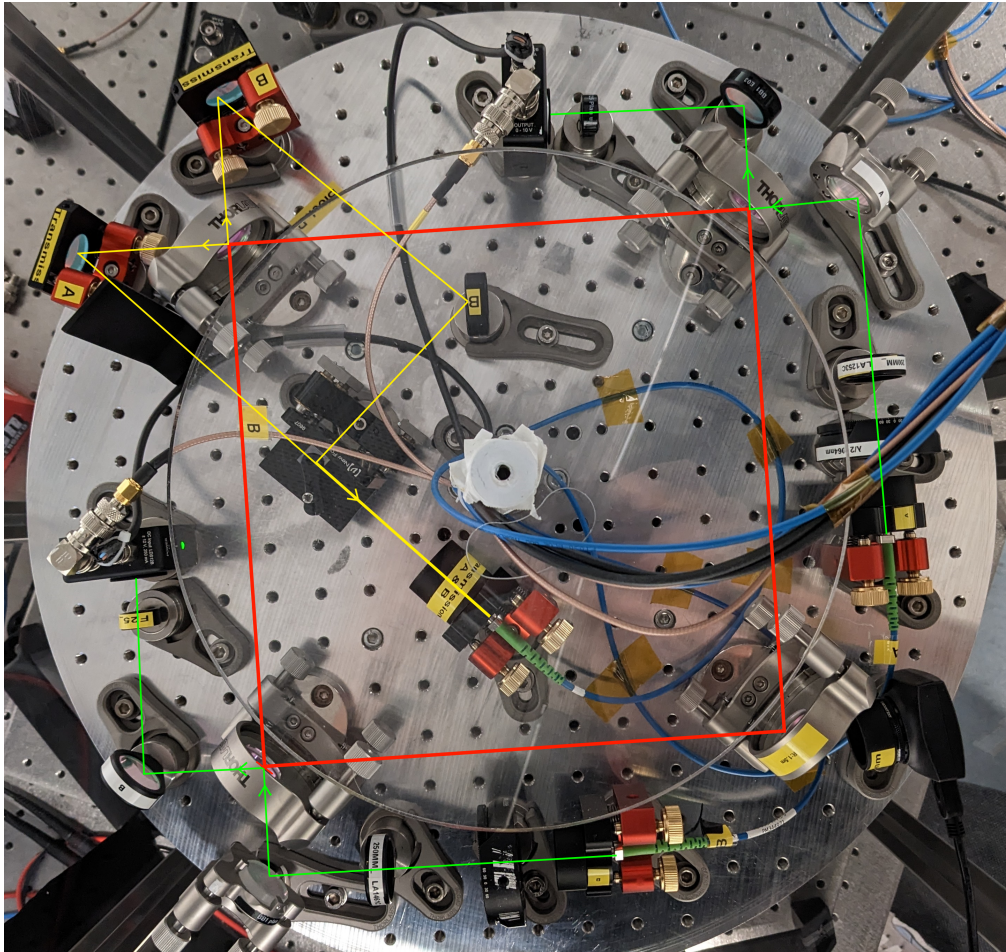


Figure 16: Photo of the gyroscope lab experiment setup on the rotation table. Gyroscope cavity: red. Incoupling and observation of the reflection: green. Observation of the transmission: yellow.

5 The lab course

5.1 Homework preparation

Prepare the following tasks at home for the first day of the lab course experiment. Bring your experimentally obtained data and the associated analysis with you – a printout of the relevant plots and a few key points with the relevant results is sufficient. Be prepared to discuss your results. Later include the analysis into your final report.

To familiarize ourselves with gyroscopes and their performance, we will use the gyroscopes that we all have in our pockets: the ones built into state-of-the-art cell phones. These are usually vibrating structure gyroscopes in shape of a micro-electro-mechanical system (MEMS) that utilize the Coriolis force action on a vibrating mass structure – a kind of tuning fork. Together with an accelerometer they for instance allow three-dimensional motion tracking for navigation, games and other applications.

Task I: Getting started Install the phyphox app (<https://phyphox.org>, made by RWTH Aachen University) on your phone⁶, select the Gyroscope function, and get to know the basic functions:

- What is the orientation of the three gyroscopes (x , y , z)? Which sense of rotation is denoted as positive/negative? Make a sketch of your phone and denote the rotation axes and senses of rotation relative to it.
- How can the rotation rates be saved and transferred to a computer for analysis? Try it.
- How fast can you spin your phone (without breaking it)? Be creative!

Task II: Allan deviation Now, position your cell phone onto a very quiet surface, such as the floor of your basement. For later it might be helpful to align one of the axis orthogonal to the rotation axis of earth.

- Take an extended time series of about an hour and display it graphically.
- Which frequency components do you observe? For all axes generate a noise spectrum (a Fourier transform, FFT) of your data. Display your results in a log-log plot.
- Calculate the Allan deviation σ_{ad} for all three axes as described in section 3.4 above and display it in a log-log plot. Select time intervals τ spanning from the sampling rate to the longest time possible. At what time does the stability turn over again, that is: when does the drift become larger than the stability?

⁶Contact the tutors in advance if you happen to not have access to a smartphone with this functionality.

- Identify the shot-noise time interval and extract the gyroscopes shot-noise limited sensitivity \mathcal{A} for all axes by fitting Equation (16) to your data. How does this compare to the rotation rate of Earth?

Hints: For calculating the Allan deviation you might need to filter out (high frequency) noise in your measurement that can appear when disturbing your phones gyroscope with your hands at the beginning or end or even just when walking by. You can try out the time automatic to eliminate disturbances at the beginning and end of your measurement. Take care about the units of the Allan deviation, we are dealing with frequency data!

Task III: Earth rotation rate

Let's try to measure the rotation rate of Earth:

- Place your phone on the floor and measure for a reasonable amount of time, guided by the results of the Allan deviation analysis in Task II. Then flip your phone and measure again. Subtracting these two measurements will allow you to remove systematic offsets of the gyroscope. You can also flip your phone a couple of times up and down, this will allow you to remove any long-term drifts. Be creative!
- Display your data graphically.
- Extract the rotation rate by subtracting the temporal averages of the two phone orientations. Guided by the results of Task II, which uncertainty do you need to assign here?
- Which value for the rotation rate of earth do you obtain? Which values do you expect for your three sensors? Does this value make sense? If not, how can it be explained?

Hints: You can try out the time automatic to eliminate disturbances and to time your flips. Take the flipping time into considerations when choosing a measurement strategy. Take care about the orientation of your phone with respect to the rotation axis of Earth!

5.2 Laboratory tasks

The following tasks are part of the two-day on-site laboratory course. You will get a thorough introduction to the laboratory optics and electronics by the tutor. Some of the steps might require a preparation of the tutor, do not attempt any steps that are not described here neither discussed on-site with the tutor! The optical setup around the cavity is very sensitive to misalignment, do not touch any optics without your permission!

Disclaimer: The lab course is brand new, so there might be problems appearing. The lab manual is also not fail-proof. **Contact the tutor for any potential questions and uncertainties!** A failure of lab hardware that was not deliberately caused by the student(s) themselves, will not negatively affect the grading of the lab course; prerecorded

measurement data can be provided if necessary.

To bring: The data taken in the lab course experiment will be recorded on a oscilloscope; for that **bring a USB stick** to take the data home! If you like to do data analysis in parallel to the laboratory experiment you might bring a computer with you.

Time management: In the following, all tasks that are part of your analysis and do not necessary need to be done on the two days of the experiment are marked. Check your data rigorously for later analysis, but focus on the experimental part during your stay in the lab.

(Task A): Operation of the gyroscope You will get an introduction to all relevant tools and parts through the tutor.

- Familiarize yourselves with the experiment.
- Record the cavity resonances and lock the first arm to the cavity:
 - Switch on the laser, the laser lock box and the AOM driver. Scan the laser over the cavity resonances, and record one of the cavity reflection signals using the photodiode preinstalled on the rotating table via the oscilloscope. Set the frequency scan offset and span using the laser lock box (Moglabs FSC) to see at least three neighboring resonances together with their pairs of sidebands.
Analysis: Assign a frequency axis to your data using the known sideband frequency and determine the free-spectral-range $\delta\nu_{\text{FSR}}$ and cavity perimeter P from the recorded spectrum. Take care when assigning the frequency axis, the laser scan does not necessarily produce a linear frequency sweep in time. Consider this in your analysis.
 - Generate an error signal of arm A by mixing the photodiode signal with the EOMs modulation frequency. Record a zoomed in error signal when scanning the cavity. *Analysis:* Try to estimate the slope of the PDH error signal by fitting a linear function to part of the signal. Why is this not really possible?
 - Connect the error signal to FSC and look at the error signal monitor outputs. Adjust the offset of both the slow and fast error signal, such that the resonance is at zero. Adjust the sign of the two loops (you need to readjust the offset) until you can lock the laser using the fast and slow part of the FSC control box. Watch the locks stability against environmental disturbances (knocking on the desk, clapping, ...) and optimize the locks PID parameters by watching the standard deviation of the fast and slow loops error signal when being locked (the tutor will help if necessary). Use the fiber-coupled transmission photodiode and the camera on the rotation table to monitor the cavity transmission to help you assess the lock quality.

- Record a camera picture of the cavity transmission when being locked. *Analysis:* Comment the picture in the context of section 3.3.1.
- Measure the cavity finesse via the cavity ring-down technique:
 - Lock one of the beams to the cavity and monitor the other beam directions cavity transmission using the fiber-coupled photodiode on the laser table breadboard.
 - Set the trigger of the oscilloscope (picoscope) to the photodiode channel and an appropriate level height. It might help to set the trigger mode to single. Then switch off the respective laser beam using the front panel control of the AOM driver. You should see the exponential decay as described in Equation (16). *Analysis:* Apply a appropriate curve fit to your data; extract ring down time, cavity finesse and a value for the cavity mirror reflectivity (assuming all mirrors are equal).
 - Get some statistics by the repeating cavity-ring-down measurement at least 10 times. It might be convenient to set the trigger mode to repeating.
- Lock the second arm of the cavity through the AOM:
 - Lock the laser to the first arm. Then rotate the table to observe a deviation from zero in the error signal of the other arm.
 - Lock the second arm to the cavity via the AOM drivers built-in control box. (Instructions will be given by the tutor.) Adjust the setpoint / offset in the AOM software such that the respective error signal does not jump when locking the AOM to the stationary (=not rotating) cavity.

(Task B): Measurement of the scale factor

- Contact the tutor to check your current status before you continue.
- Set the gyroscope table into rotation and measure its rotation rate via the rotary encoder. You can use the oscilloscopes (picoscope) math channel functionality (choose freq(CH) with CH being the appropriate oscilloscope channel) to get a direct monitor for the encoder rate. How does this translate to the tables rotation rate?
- Monitor the beat signal between the two arms via the RF mixer that mixes the two AOM driving signals. Their frequency difference corresponds to the Sagnac frequency if everything is set up correctly.
- Measure the scale factor of the gyroscope for 5 different rotation speeds. Monitor and record both the rotary encoder as well as the Sagnac beat while rotating the table using the motor. Set these rotation rates thoughtfully and watch the laser locks stability. *Analysis:* The scale factor is the ratio between the rotation rate and the Sagnac frequency. Extract rotation rate and Sagnac frequency from your

data; for averaging, select time windows in which the rotation rate is stable. Plot them against each other and apply a linear interpolation. What value did you expect from your previous measurements?

Hint: If the laser falls out of lock during your measurement (and it probably will!), just relock and continue recording. You will be provided a secondary oscilloscope to monitor the laser lock while using the Picoscope to record the beat signals and rotary encoder. Filter your data for these lock failures later.

(Task C): Allan deviation

- Choose a small yet stable rotation rate, and measure the Sagnac frequency for a time series as long as possible. Use this data set to generate the Allan deviation.
- *Analysis:* Show the Allan deviation in a log-log plot as done already for the homework. Therefore convert the measured Sagnac frequency to a rotation rate. Also identify the time range of pure shot-noise limitation and extract the gyroscopes sensitivity via an appropriate linear fit via Equation (16). Also compare to the theoretical expectation of Equation (4) assuming that $1\text{ }\mu\text{W}$ of optical power is available for detection. Try to explain.

Hint: Try to record as long as the lock allows you. Be careful when adding multiple datasets and filtering out lock failures in your data. These jumps in the signal height can lead to nonphysical signatures in your Allan deviation, but you can try to eliminate them.

(Task D): Measuring the Earth's rotation rate

- *Calculate:* Assuming realistic experimental parameters of wavelength λ , cavity enclosed area A , and beam diameter $d = 300\text{ }\mu\text{m}$, estimate the gyroscopes lock-in threshold. Although your estimation is certainly only an order-of-magnitude estimation, explain why the present setup does not allow to directly observe the Earth's rotation rate.
- **Optional:** The Earth's rotation rate could in principle be obtained from sufficiently precise measurements at a number of different finite rotation rates. Adding an artificial “offset” is called dithering and common to all commercially available fiber-optic gyroscopes used in industry and aviation. Devise a measurement strategy and explain how one could measure the Earth's rotation rate using this setup.

References

- [1] T. Artz, *Determination of Sub-daily Earth Rotation Parameters from VLBI Observations*, PhD thesis (2011).
- [2] K. U. Schreiber and J. R. Wells, *Large ring lasers for rotation sensing*, Rev. Sci. Instrum. **84**, 041101 (2013).
- [3] W. Z. Korth, A. Heptonstall, E. D. Hall, K. Arai, E. K. Gustafson, and R. X. Adhikari, *Passive, free-space laser gyroscope*, Classical Quantum Gravity **33**, 035004 (2016).
- [4] K. Liu, F.L. Zhang, Z.Y. Li, X.H. Feng, K. Li, Z.H. Lu, K U. Schreiber, J. Luo, and J. Zhang, *Large-scale passive laser gyroscope for Earth rotation sensing*, Optics Letters **44**, 2732 (2019).
- [5] G. Rizzi and M. L. Ruggiero, *A Direct Kinematical Derivation of the Relativistic Sagnac Effect for Light or Matter Beams*, General Relativity and Gravitation **35**, 1572 (2003).
- [6] E. D. Black, *An introduction to Pound-Drever-Hall laser frequency stabilization*, American Journal of Physics **69**, 79 (2001).
- [7] D. Meschede, *Optik, Licht und Laser*, Vieweg+Teubner Verlag (2008).
- [8] C. Wind, *A passive, free space laser gyroscope*, Master thesis (2021).
- [9] Moglabs, *Pound-Drever-Hall Locking with the FSC*, Application Note AN002, <https://www.moglabs.com/support/appnotes/an002-pdh-r2.pdf>
- [10] Moglabs, *Fast Servo Controller (FSC)*, Manual, Version 1.0.1, https://www.moglabs.com/products/laser-electronics/fast-servo-controller/MOGLabs_FSC_manual_v1.0.1.pdf,
- [11] E. A. Whittaker, M. Gehrtz and G. C. Bjorklund, *Residual amplitude modulation in laser electro-optic phase modulation*, J. Opt. Soc. Am. **B 2**, 1320 (1985).